Balance of physical effects causing stationary operation of Fourier domain mode-locked lasers

Sebastian Todor,[1,*] Benjamin Biedermann,[2] Robert Huber,[2] and Christian Jirauschek[1]

[1]*Institute for Nanoelectronics, TU München, Arcisstraße 21, D-80333 Munich, Germany*
[2]*Lehrstuhl für BioMolekulare Optik, Fakultät für Physik, Ludwig-Maximilians-Universität München, Oettingenstr. 67, D-80538 Munich, Germany*
**Corresponding author: Todor@tum.de*

Received October 14, 2011; revised November 30, 2011; accepted November 30, 2011; posted December 1, 2011 (Doc. ID 156468); published March 16, 2012

We present a detailed analysis of the optical field dynamics in a Fourier domain mode-locked (FDML) laser. We employ a numerical simulation based on the FDML evolution equation, describing the propagation of the optical light field. The temporal evolution of the instantaneous power spectrum at different points in the laser cavity is investigated. The results are carefully validated against experimental data, yielding good agreement. Deeper insight is gained into the role of the physical effects governing FDML dynamics, such as gain recovery and linewidth enhancement in the semiconductor optical amplifier, dispersion and self-phase modulation in the optical fiber, and the sweep filter action.

OCIS codes: 140.3600, 140.3430, 170.4500.

1. INTRODUCTION

Recently, there has been a growing interest in swept laser sources with high sweep rates, driven by various applications, such as optical coherence tomography (OCT) [1,2] and sensing applications [3]. Conventional tunable lasers are inherently limited in their sweep frequencies due to the comparatively long buildup time of the lasing action within the cavity [4]. In Fourier domain mode-locked (FDML) lasers [5], this limitation is not present, enabling very high sweep frequencies. This is achieved by employing a tunable intracavity bandpass filter that is driven synchronously to the round trip time of the light in the laser cavity. Therefore, lasing does not have to build up repetitively but instead is only limited by the response time of the tunable bandpass filter. A record sweep rate of above 5 MHz has been achieved using a 325 kHz FDML laser and multiplying the sweep repetition rate by the so-called buffering technique [6–8]. Besides restrictions in the tuning speed of the filter, no fundamental sweep speed limitations arise in FDML. In principle, many types of rapidly tunable filters can be applied, such as sampled grating distributed Bragg reflector based filters [9], rotating polygon mirror based filters [10], filters based on resonant galvanometer mirrors [11], micro-electro-mechanical systems (MEMS)-based tunable Fabry–Perot filters [12], etc. Typical instantaneous linewidths of <0.1 nm, corresponding to a coherence length of several millimeters up to centimeters [13], together with the high sweep rates currently make the FDML laser the system of choice for many high speed OCT and sensing applications [6,13–28]. To date, other very promising approaches that do not suffer from the inherent limitation of sweep speed have not achieved the combination of speed, tuning range, low noise, and output power. A 5 MHz swept source realized by temporally stretching an ultrashort laser pulse achieved an extremely wide tuning range but had too high noise for high quality OCT imaging [29]. A wavelength swept amplified spontaneous emission (ASE) source achieved >300 kHz tuning rate but also exhibited too much noise to fully achieve shot noise limited detection in OCT [30,31]. Tunable VCSELs with a MEMS mirror achieve up to 760 kHz sweep rate [32–34] with very good coherence length but smaller sweep range and output power than FDML lasers. Classical swept lasers for OCT have been demonstrated at sweep rates up to 400 kHz [35].

It has been shown that FDML is a real stationary laser operating regime [36], not only a form of ASE light source [30,31]. However, it is not yet fully understood how the physical effects governing the FDML dynamics, such as the gain and sweep filter action, interact to form the steady state light field in the laser cavity. In the following, we study in detail the steady state evolution of the cavity field, identifying the role of each optical element in the laser cavity for the stationary operation. For our analysis, we employ our recently developed theoretical model of FDML operation, which has been shown to yield both the instantaneous optical power and power spectrum in good agreement with experiment [36,37]. Based on this model, we simulate the instantaneous power spectra at different times and at various positions within the laser cavity, isolating the effect that each of the optical cavity elements has on the laser dynamics. From these time and space resolved data, a deeper understanding of the steady state FDML operation can be obtained.

The paper is organized as follows: In Sections 2 and 3, the experimental setup and simulation approach are described, and the effects leading to a broadening of the measured lineshapes are discussed. In Section 4, we theoretically and experimentally investigate the spatiotemporal evolution of the light field in the laser cavity by simulating the instantaneous lineshape profiles at different times and positions in the laser cavity. The obtained results provide an improved insight into the FDML dynamics.

2. EXPERIMENTAL SETUP

The laser setup is based on a polarization maintaining (PM) sigma ring geometry, as shown in Fig. 1. We use a solid state optical amplifier (SOA, Covega Corp., "BOA 1132") as a gain medium, with the gain maximum located at 1320 nm. The two isolators (ISO) before and after the SOA ensure unidirectional lasing. Using a polarization beam splitter (PBS), the light is coupled into 1.7 km of single mode fiber (SMF) serving as a delay line, and it is back-reflected, employing a Faraday rotating mirror (FRM). This leads to an effective cavity length of 3.4 km, corresponding to a round trip time of $T = 17.32\ \mu$s. The sweep filter is driven synchronously to the cavity round trip time, i.e., with a sweep rate of 57.7 kHz. A tunable bandpass filter (FFP-TF, Lambda Quest, LLC.) with a bandwidth of 0.156 nm is used, driven sinusoidally with a sweep range of 105 nm around 1320 nm. The light can be coupled out at three different positions within the laser cavity, numbered 1 to 3. This enables us to probe the light field at different positions within the laser cavity. In order to extract the instantaneous power spectrum, the laser light from any of the three outcouplers is fed into an electro-optical modulator (EOM), as shown in Fig. 1(a). The EOM is also synchronized to the round trip time and is triggered with pulses of 1.6 ns length, serving as time gate for the laser light. The optical spectrum analyzer then extracts the instantaneous power spectrum from these gated light pulses. Compared to the full round trip time, this pulse duration corresponds to an almost "instantaneous" spectrum. However, there occur several effects that can broaden the measured instantaneous linewidth compared to the theoretical value by up to 4 GHz [37,38]. The broadening of the spectra due to the finite time gating of 1.6 ns, resulting in increased measured linewidths due to the sweep filter dynamics and Fourier broadening, has been taken into account in our simulations.

3. SIMULATION

Starting from the evolution equation for the field envelope $u(z,t)$ in the FDML laser [36],

$$\partial_z u = [g(\omega_0)(1 - i\alpha) - a(\omega_0) + i\omega_0^2 D_2 + i\omega_0^3 D_3 - iD_2\partial_t^2 + i\gamma|u|^2 - a_s(i\partial_t)]u, \quad (1)$$

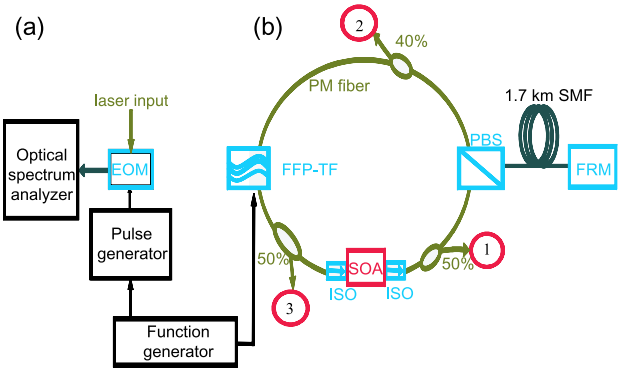

Fig. 1. (Color online) (a) Setup for the measurement of the instantaneous linewidth using an electro-optical modulator (EOM) and an optical spectrum analyzer. (b) FDML laser setup with three outcouplers (numbered 1 to 3), where light is extracted for the linewidth analysis.

the laser is modeled using a split-step Fourier algorithm [39]. The very large time-bandwidth product associated with the frequency-swept light field is drastically reduced in Eq. (1) by using the swept-filter reference frame [36]. Because the 0.156 nm wide filter blocks all light far outside the passband, not the entire spectral sweep bandwidth has to be taken into account; instead, a spectral window of 2.8 nm around the filter center frequency is here considered, corresponding to 500 GHz. Since the temporal simulation window is adapted to the round trip time $T = 17.32\ \mu$s due to the implicit periodic boundary conditions of the algorithm [36], the frequency resolution is $\Delta f = 1/T = 57.7$ kHz. Thus, about 8 million grid points are used, as compared to 300 million without switching to the swept-filter reference frame. All relevant physical effects are contained in the simulation, such as the self-phase modulation γ, dispersion effects (second and third order dispersion, D_2 and D_3), and the linewidth enhancement α [40] of the gain medium. The coefficients $a(\omega_0)$ and $g(\omega_0)$ represent the frequency-dependent loss and gain, respectively, and are functions of the time dependent sweep filter center frequency $\omega_0(t)$; g also accounts for gain saturation effects. The term $-a_s(i\partial_t)u$ represents the sweep filter action.

In Fig. 2(a), $\omega_0(t)$ as well as the corresponding wavelength $\lambda(t)$ is shown, and in Fig. 2(b) the simulated power after the SOA is displayed as a function of time. The power spectrum in the swept-filter reference frame is given by $|U(z,f)|^2$, where $U(z,f)$ denotes the Fourier transform of $u(z,t)$, and f is the frequency coordinate relative to the center frequency of the sweep filter. By dividing the round trip time into subintervals and Fourier transforming the output power in each of these intervals separately, we can examine the temporal evolution of the instantaneous power spectrum. The number of the intervals should be sufficiently high to obtain a good temporal resolution. On the other hand, in order to avoid Fourier broadening of the instantaneous power spectra, the subintervals should not be too short. We choose 16 subintervals with a duration of 1.08 μs each, so that the effect of Fourier broadening is still negligible.

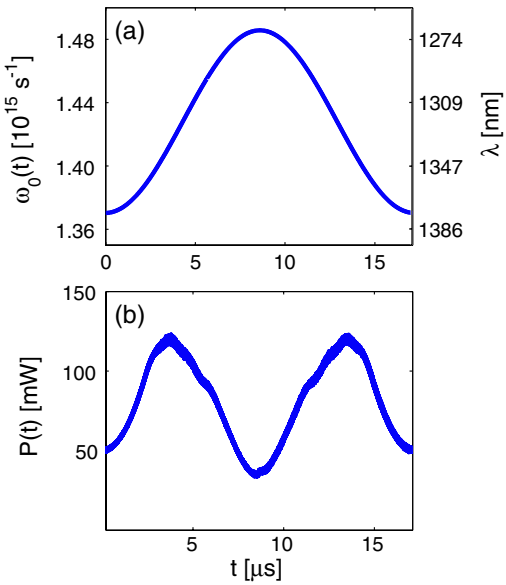

Fig. 2. (Color online) (a) Time dependent sweep filter center frequency and wavelength and (b) simulated power over time.

The finite time-gating of 1.6 ns (FWHM) in the measurement setup in Fig. 1(a) leads to Fourier broadening, as well as spectral broadening due to the sweep filter dynamics during the measurement. As discussed above, both effects can be suppressed in the simulation: The time gating is chosen long enough as to avoid Fourier broadening, and the field envelope u in Eq. (1) is described in the swept filter reference frame where the frequency axis moves along with the sweep filter center frequency. However, for direct comparison of the simulated and the experimentally measured spectra, the effects of finite time gating should be considered in the simulation. For the implementation of these effects, the relation between the complex field envelope u in the swept filter reference frame and the untransformed envelope function A has to be used [36],

$$u = A \exp\left(i \int^t \omega_0(t')\mathrm{d}t'\right). \tag{2}$$

The sweep filter is driven by a cosine function, given by $\omega_0(t) = -(\Delta\omega/2)\cos(2\pi t/T)$. For a measurement at time t_0, we can use a Taylor expansion and write the integral in the exponent of Eq. (2) as

$$\int_{t_0}^{t} \omega_0(t')\mathrm{d}t' = \omega_0(t_0)(t-t_0) + \frac{1}{2}\frac{\partial\omega_0}{\partial t}\bigg|_{t=t_0}(t-t_0)^2 + \ldots, \tag{3}$$

where the first term induces merely a spectral shift in the Fourier domain and is not further considered, while the second term induces spectral broadening. We therefore obtain for the gated field envelope the relation

$$A = u \cdot \exp\left(-\frac{(t-t_0)^2}{2\sigma^2} - \frac{i}{2}\frac{\partial\omega_0}{\partial t}\bigg|_{t=t_0}(t-t_0)^2\right). \tag{4}$$

with the Gaussian pulse duration $\sigma = 1.6\ \mathrm{ns}/2/\ln(2)^{1/2} = 0.961$ ns. The power spectrum is given by $|A(z,f)|^2$, where $A(z,f)$ denotes the Fourier transform of $A(z,f)$, and the frequency axis is here centered around the sweep filter center frequency at time t_0.

An additional effect that has to be considered is that the experimentally obtained power spectra are averaged over several thousands of round trips, thus eliminating fluctuations which arise during the short gating time. In order to take into account this effect, we average the simulated gated spectra over 20 nonsubsequent round trips by evaluating every tenth spectrum, starting from round trip 900 to ensure convergence of the simulation. This proves sufficient for eliminating fluctuations. On the other hand, averaging turns out to be unnecessary for the simulated spectra obtained without gating, since their fluctuations are eliminated due to the much longer time intervals over which the spectra are extracted. Furthermore, the optical spectrum analyzer used in the experimental setup shown in Fig. 1(a) has a finite resolution of 20 pm, corresponding to a spectral width of 3.5 GHz at 1310 nm. To imitate this effect, the obtained numerical spectra are smoothened over 4000 points. The power dependence is not investigated here, but instead power and gain levels typical for OCT imaging applications are chosen.

In Fig. 3, the simulated instantaneous power spectrum after the SOA at $t = 5.3$ μs is shown for gating and averaging considered (dotted curve) and without taking these effects into account (dashed curve), and compared to the experimental data (dash-dotted curve). The FWHM values are 13.77 GHz, 10.13 GHz, and 15.81 GHz, respectively. As can be seen, the consideration of the time gating in the simulation is essential for a precise comparison to experiment. Without the inclusion of these effects, the simulated FWHM linewidth does not match the experimental data very well, as expected. Further simulations show that by substantially reducing dispersion and self-phase modulation within the cavity, and by implementing narrower sweep filters, the instantaneous linewidth can be considerably reduced. Preliminary results indicate that in the optimum case, linewidths down to the inverse duration of one sweep direction could be achieved; in this case this corresponds to 100 kHz.

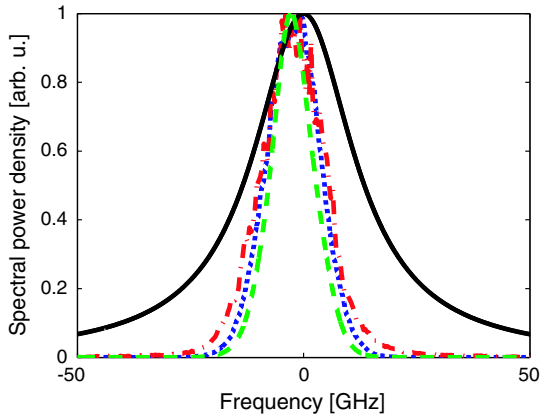

Fig. 3. (Color online) Instantaneous power spectrum at $t = 5.3$ μs after the SOA for the simulation with gating considered (dotted curve), for the simulation without gating (dashed curve), and as obtained from experiment (dash-dotted curve). The sweep filter transmission (solid curve) is shown for comparison.

4. TEMPORAL AND SPATIAL EVOLUTION OF THE OPTICAL CAVITY FIELD

In Fig. 4, the simulated temporal evolution of the instantaneous power spectra is shown after the SOA. The spectra change with time but show an overall shift toward negative frequencies. In this section, we theoretically and experimentally investigate the temporal evolution of the spectral properties, as well as the spatial evolution along the resonator axis.

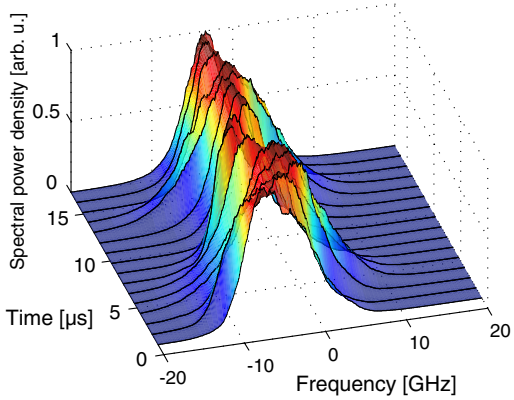

Fig. 4. (Color online) Simulated temporal evolution of the instantaneous power spectrum after the SOA over a full round trip without gating included.

In particular, we investigate how the interplay of the various effects leads to the formation of a steady state light field.

A. Discussion of the Spectral Shaping Effects

FDML simulations indicate that the temporal and spatial evolution of the laser field, here characterized by its instantaneous power spectrum, is dominated by the gain dynamics including linewidth enhancement, the dispersion and self-phase modulation in the optical fiber, and the sweep filter action [36,37]. In the following, we investigate how each of these effects contributes to the spectral shaping of the light field.

First, we analyze the contribution of the linewidth enhancement factor to the spectral shaping, which has been observed to cause a shift of the power spectral peak to lower frequencies [37]. This effect is here more closely investigated. We can solve Eq. (1) keeping only the term associated with the optical gain, and obtain

$$u = u_0 G^{(1-i\alpha)/2}, \tag{5}$$

where the total power gain is related to the gain coefficient by integrating over the length of the gain medium, $G = \exp[2\int g(\omega_0)\mathrm{d}z]$. For the modeling of the gain dynamics, we have to consider both the saturation behavior and the spectral dependence [36], which is done by using an ansatz

$$G(t) = \frac{G_0[\omega_0(t)]}{1 + P_{\mathrm{av}}(t)/P_{\mathrm{sat}}[\omega_0(t)]}. \tag{6}$$

The spectral dependence enters through the frequency-dependent peak gain G_0 and saturation power P_{sat}. The saturation is modeled based on a quasi-instantaneous gain saturation approach [36], accounting for the finite carrier lifetime in the SOA that governs the gain recovery dynamics, assuming a typical value $\tau_c = 380$ ps [41]. In this approach, the saturation level of the gain at a time t is not directly determined from the instantaneous optical power $P(t)$ but rather based on a moving average value

$$P_{av}(t) = \tau_c^{-1}\int_{-\infty}^{t} P(\tau)\exp[(\tau - t)/\tau_c]\mathrm{d}\tau. \tag{7}$$

In this way, relaxation processes in the gain medium, which lead to a noninstantaneous gain recovery for changes of the optical power on timescales faster than the carrier lifetime, can be adequately taken into account [36]. Such fast changes can arise due to the complex FDML dynamics themselves, and are also induced by ASE and other noise sources. For the simulated optical power shown in Fig. 2(b), these high frequency contributions are largely suppressed because of the smoothing applied there, corresponding to a sampling rate of 500 MHz to imitate the experimental measurement setup. However, these contributions give rise to a broadened instantaneous linewidth, as shown in Fig. 3. We investigate the influence of the linewidth enhancement factor, taking a Gaussian spike $P_0 = u_0^2 = P_g \exp(-t^2/T_g^2)$ where the peak power is set to $P_g = 10P_{\mathrm{sat}}$ and T_g is chosen so that the corresponding power spectrum has a FWHM value of 10 GHz, similarly to the observed instantaneous linewidths [37]. In Fig. 5(a), the Gaussian spike $P_0(t)$ and the moving average value $P_{\mathrm{av}}(t)$ obtained from Eq. (7) for $\tau_c = 380$ ps is shown. As can be seen, the relaxation process induces an asymmetry in the form of a slow decay of $P_{\mathrm{av}}(t)$. In Fig. 5(b), the power spectrum of the Gaussian input pulse is shown along with the output power spectrum after the gain medium, obtained with Eq. (5) for $\alpha = 5$. The peak of the output spectrum is shifted by −3.6 GHz. Further simulations show that the shift is almost exclusively due to the linewidth enhancement, i.e., the imaginary part of the term $(1 - i\alpha)$ in Eq. (5), and not the real part corresponding to the amplification. In other words, the combination of linewidth enhancement and the recovery dynamics in the gain medium leads to the spectral red shift.

Now we focus on the dispersive effect in the optical fiber. In previous simulations we found that if the sweep rate is detuned with respect to the round trip time of the light within the cavity, the third order dispersion D_3 causes a spectral asymmetry, which is however greatly reduced for the non-detuned case considered here [37]. In the following, we investigate the time dependent influence of dispersion for no detuning. Considering only the relevant terms in Eq. (1), we can obtain a closed analytical solution. For the propagation through a dispersive fiber of length L, the field envelope at the end of the fiber is given by

$$u(z + L) = u(z)\exp\{\mathrm{i}[\omega_0^2(t)D_2 + \omega_0^3(t)D_3]L\} = u(z)\exp[\mathrm{i}\phi(t)]. \tag{8}$$

Here we have neglected the term $-iD_2\partial_t^2 u$, which by itself does not affect the power spectrum. As described in Section 3, the instantaneous power spectrum at a time t_0 is obtained by dividing the round trip time into subintervals and Fourier transforming the output power in the corresponding interval

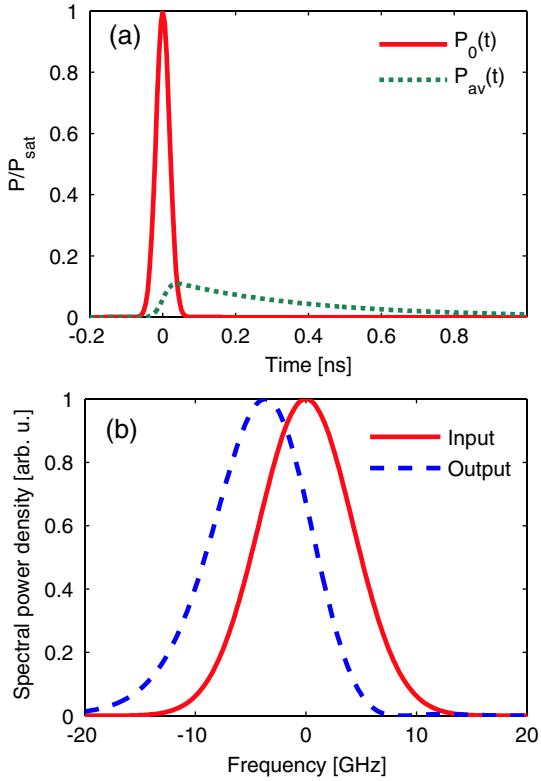

Fig. 5. (Color online) (a) Gaussian input pulse and the corresponding averaged power obtained from Eq. (7) as a function of time. (b) Power spectrum of the Gaussian input pulse and output power spectrum after the gain medium.

separately. In the subinterval centered around t_0, the exponent in Eq. (8) can be approximated by a Taylor expansion

$$\phi(t) \approx \phi(t_0) + \partial_t\phi(t_0)(t - t_0) + \ldots \tag{9}$$

Though the zeroth order term $\phi(t_0)$ just represents a constant phase shift, the first order term contains $\partial_t\phi(t_0)$, which corresponds to the instantaneous frequency, inducing a spectral shift by the amount

$$\delta f = -\partial_t\phi(t_0)/(2\pi) = -\frac{1}{2\pi}[2D_2\omega_0(t_0) + 3D_3\omega_0^2(t_0)]\partial_t\omega_0(t_0)L \tag{10}$$

in the Fourier domain. It should be pointed out that dispersion as a linear effect does not change the photon energy but causes an additional delay of the optical field in the fiber. Because of the sweep dynamics, this re-timing of the optical field leads to an additional spectral shift of the instantaneous power spectrum with respect to the sweep filter center frequency, as described by Eq. (10). In Fig. 6, the spectral shift δf according to Eq. (10) as a function of t_0 is shown for a single propagation through the optical fiber with $D_2 = -276$ fs^2/m, $D_3 = 12183$ fs^2/m, and $L = 3400$ m. Since the center wavelength in our simulation is 1320 nm, which is close to the zero dispersion point $D_2 = 0$, the influence of D_3 is dominant.

The self-phase modulation in the optical fiber is well known to induce spectral broadening [39]. For a very slowly varying output power level, as in the ideal FDML laser, this effect might be negligible. However, in real operation, the optical power exhibits high frequency fluctuations as discussed above. As a consequence, self-phase modulation has a considerable influence on the instantaneous power spectrum. In the following, we investigate this effect, using a Gaussian spike as a model for optical power fluctuations. Considering only the relevant term in Eq. (1), we obtain the solution

$$u(z + L) = u(z)\exp(\mathrm{i}\gamma|u(z)|^2L). \tag{11}$$

The effect of the self-phase modulation is illustrated in Fig. 7 for $\gamma = 0.00136$ W/m and again a fiber length of $L = 3400$ m, assuming the same Gaussian input pulse as in Fig. 5, here with a peak power of 200 mW. Though self-phase modulation does not induce a frequency shift, it causes spectral broadening.

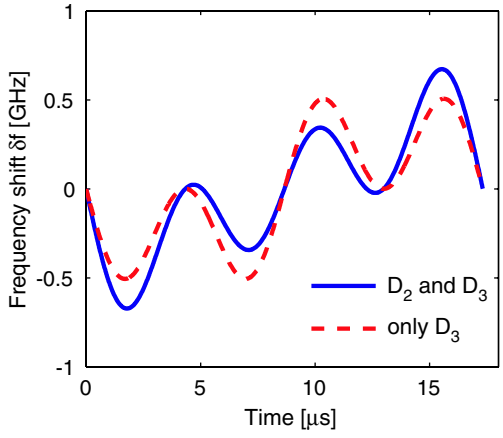

Fig. 6. (Color online) Temporal dependence of the frequency shift caused by the fiber dispersion.

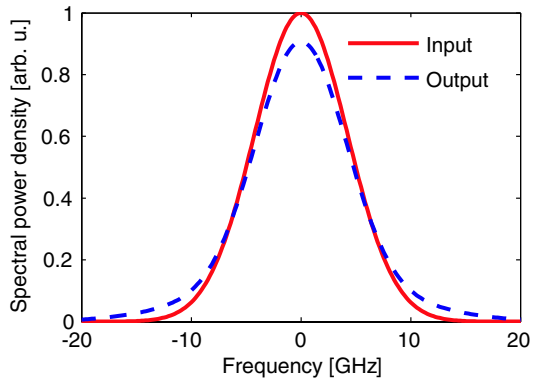

Fig. 7. (Color online) Power spectrum of the Gaussian input pulse and output power spectrum after self-phase modulation.

Next we investigate the effect of the sweep filter, which, as we will show in the following, acts as a bandpass filter and balances the frequency shift induced by the dispersion and the linewidth enhancement. We solve Eq. (1) in frequency domain, keeping only the term associated with the sweep filter and using $\omega = 2\pi f$, and obtain the pulse envelope in Fourier domain

$$U(\omega) = t_s(\omega)U_0(\omega). \tag{12}$$

The sweep filter is modeled as a lumped optical element, where the transmission characteristic is related to the sweep filter coefficient by integrating over the length of the sweep filter [36], with

$$t_s(\omega) = \exp[-\int a_s(\omega)\mathrm{d}z] = T_{\max}^{1/2}/(1 - 2\mathrm{i}\omega/\Delta). \tag{13}$$

Here, we choose $\Delta = 0.169$ ps^{-1}, corresponding to a Lorentzian filter with an FWHM bandwidth of 0.156 nm. The effect of the sweep filter is illustrated in Fig. 8 for the same Gaussian input pulse as in Fig. 5 but shifted by −10 GHz relative to the sweep filter center frequency. The low-frequency wing of the spectrum is "cut off" by the sweep filter, which induces an effective shift of the output spectrum toward higher

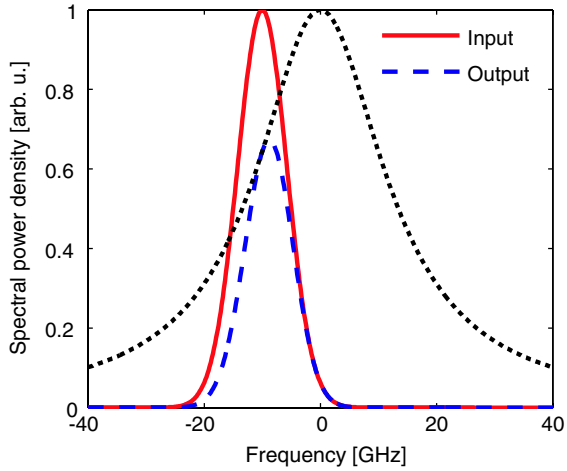

Fig. 8. (Color online) Power spectrum of the Gaussian input pulse and output power spectrum after the sweep filter. The sweep filter transmission (dotted curve) is shown for comparison.

frequencies. Similarly, spectra centered around positive frequencies are effectively shifted to lower frequencies, thus reducing the spectral shift. Furthermore, the sweep filter acts as a bandpass, narrowing the linewidth of the instantaneous power spectrum.

Because of its complex transmission characteristic [see Eq. (13)], the filter induces not only absorption but also a frequency-dependent phase offset $\varphi = \arctan(2\omega/\Delta)$. Approximating the phase by a first order Taylor series expansion in analogy to Eq. (9), $U(\omega)$ in Eq. (12) acquires an additional linear phase, which corresponds to a delay of the optical field in time domain. Because of the sweep dynamics, this re-timing of the optical field is associated with an additional spectral shift. However, for the sweep filter parameters of the investigated laser, this time delay amounts to only 10 ps at the center and even less in the wings of the filter, corresponding to a maximum frequency shift of 30 MHz, which is much smaller than the effective shift caused by the sweep filter absorption. We have confirmed this by comparing simulations with and without considering the phase in Eq. (13), yielding very similar results and thus showing the negligible influence of these phase contributions.

The resulting instantaneous power spectra in steady state operation are thus determined by a balance between the frequency shift induced by dispersion and linewidth enhancement on the one hand, and the compensating effect of the sweep filter on the other hand.

B. Analysis of the FDML Dynamics in Steady State Operation

In order to better understand the interplay of the various optical cavity elements leading to the formation of a steady state light field, the temporal evolution of the instantaneous power spectrum at various points in the cavity is monitored. The simulation results are shown in Fig. 9 for the mean frequency and FWHM linewidth, extracted from the obtained spectra without gating. In Fig. 9(a), the temporal evolution of the mean frequency, extracted from the obtained power spectra, is shown after the SOA, the fiber, and the sweep filter. By comparing the results after the sweep filter and the SOA, it can be seen that the SOA causes a negative frequency shift at all times. This is due to the linewidth enhancement, as shown in Fig. 5. The fiber dispersion induces a negative frequency shift during the forward sweep and a positive shift during the backward sweep, as illustrated in Fig. 6. However, the linewidth enhancement dominates, leading to negative mean frequency values at all times. Finally, the sweep filter partly compensates for this negative shift, stabilizing the operation and leading to the formation of a steady state. In Fig. 9(b), the temporal evolution of the FWHM linewidth is shown, as obtained for a single round trip. The sweep filter acts as a bandpass [see Fig. 8], thus narrowing the linewidth and compensating for the broadening induced by the SOA and the fiber. The linewidth maxima coincide with the power maxima in Fig. 2(b). The reason is that the phase offset due to self-phase modulation, and thus the resulting spectral broadening, depends on the optical power, see Eq. (11). The investigated setup operates at around 1320 nm close to the zero dispersion point $D_2 = 0$. For lasers operating at different wavelengths, the second order dispersion can play a major role. To investigate this effect, simulations have been performed using the

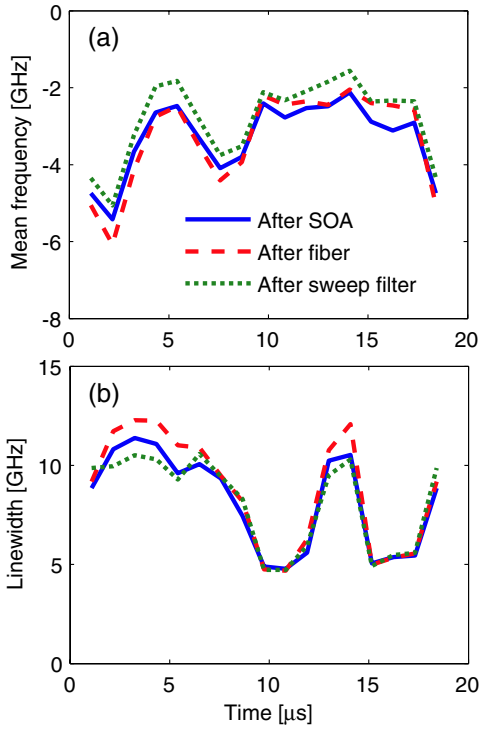

Fig. 9. (Color online) Simulation results for the temporal evolution of (a) mean frequency and (b) linewidth.

value of D_2 at 1550 nm (anomalous dispersion regime) and at 1060 nm (normal dispersion regime). In both cases the overall linewidth increases significantly, and also the linewidth change during a round trip is more pronounced. For the D_2 at 1550 nm, the instantaneous linewidth varies between 7.10 and 27.15 GHz, and similar values are obtained for the D_2 corresponding to 1060 nm.

C. Comparison to Experiment

In order to verify the validity of our simulation approach, we compare the numerical results to the experimental data. To enable a quantitative comparison, we include in our simulations the experimental effects of time gating, averaging, and limited measurement resolution, as described in Section 3. First, we extract the FWHM linewidth of the simulated and experimental spectra as a function of time. In Fig. 10, the theoretical and experimental linewidth is plotted versus time. The experimental data indicate an asymmetry of the linewidth evolution for the forward and the backward sweep, with maxima obtained at around 4.3 μs and 13.7 μs, the positions where the sweep filter speed is maximum. This trend is also confirmed for the simulations with gating included, which yield reasonable qualitative and quantitative agreement with the experiment. The simulation data without gating reveal a much smaller linewidth dependence, demonstrating that the observed maxima are mainly due to the fast sweep filter dynamics at these positions, leading to a maximum broadening effect during the finite time gating.

In the following, we compare the instantaneous power at various positions in the laser cavity. The time is fixed to $t = 5.3$ μs. In Fig. 11, the experimental (dashed curve) and theoretical (dotted curve) spectral power density is plotted after the SOA, the fiber and the sweep filter, respectively. Since the instantaneous power spectrum is measured on an

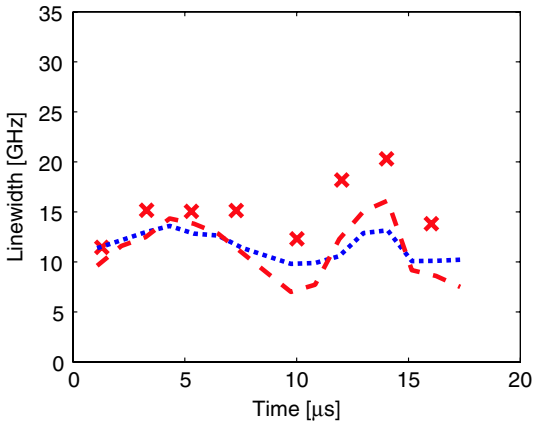

Fig. 10. (Color online) Simulated and measured temporal evolution of the linewidth. Shown are simulation results with gating considered (dashed curve) and without gating (dotted curve), as well as experimental data (crosses).

absolute frequency scale and the time dependent sweep filter center frequency at the measurement time is not known with sufficient accuracy, it is not possible to determine the frequency shift of the experimental power spectra. Thus, the frequency axis of the experimental spectra is chosen so that the experimental and simulated peak positions coincide. In Fig. 11(a), the FWHM spectral width after the SOA is 15.81 GHz for the experimental spectrum and 13.77 GHz for the simulated spectrum, respectively. The mean frequency of the simulated spectrum is located at −2.28 GHz with respect to the sweep filter reference frame. In Fig. 11(b), the spectral power density is plotted after the SMF. The FWHM is 13.82 GHz for the experimental data, and 13.83 GHz for the simulation, respectively. The simulated mean frequency shift is −2.39 GHz. Figure 11(c) shows the instantaneous power spectra after the sweep filter. Now the FWHM is 12.68 and 13.19 GHz for the experimental and theoretical data, respectively, while the simulated mean frequency shift is −1.71 GHz.

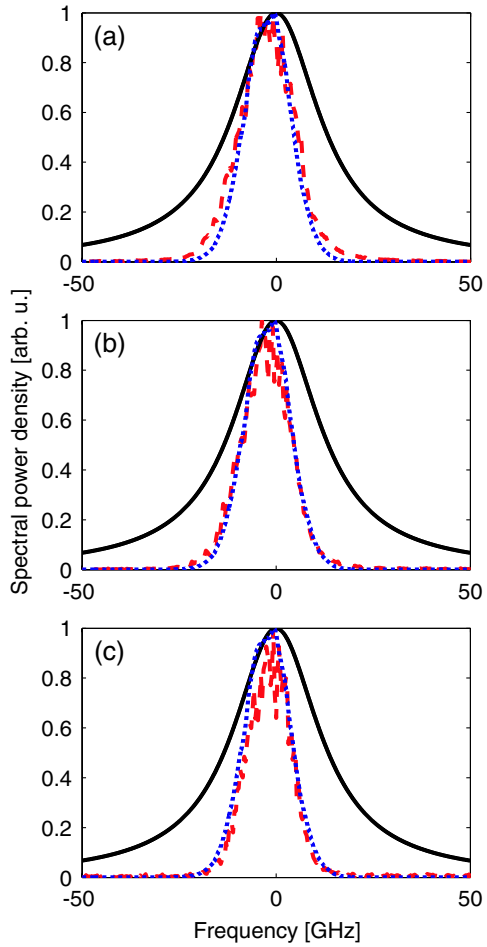

Fig. 11. (Color online) Experimental (dashed) and theoretical (dotted) instantaneous power spectra after (a) the SOA, (b) the SMF, and (c) the sweep filter at $t = 5.3$ μs. The sweep filter transmission (solid curve) is shown for comparison.

Altogether, the results displayed in Figs. 10 and 11 show good qualitative and quantitative agreement between the simulation and experiment, confirming the validity of the chosen simulation approach. The inclusion of optical gating, averaging over several round trips, and limited measurement resolution in the simulation enables us to evaluate the additional linewidth broadening caused by these effects, thus allowing for a closer comparison with experiment, and an assessment of the influence of these effects on the experimental data. Remaining deviations between theoretical and experimental results are mainly ascribed to uncertainties in some of the used laser parameters. For example, the relaxation time and linewidth enhancement factor of the SOA may deviate somewhat from the assumed typical values. Furthermore, the spectral features depend strongly on the detuning of the sweep filter with respect to the cavity round trip time [37]. While the zero detuning point can be exactly fixed in the simulation, it can only be approximately determined in the experiment based on criteria such as the maximum obtained output power.

5. CONCLUSION

In conclusion, the paper provides an answer to the question, why FDML lasers operate in a stationary regime. A quantitative analysis is given about which effects balance each other, leading to a stable spectrum and output power:

(1) A red shift of the instantaneous power spectrum toward lower frequencies is caused by the linewidth enhancement of the SOA in combination with the gain recovery dynamics. Also the dispersion induces a time dependent spectral shift. These effects are counterbalanced by the asymmetric absorption of the tunable spectral bandpass filter. For a red-shifted spectrum, the sweep filter transmission function causes an effective shift to higher frequencies by reducing the low-frequency spectral wing.

(2) Self-phase modulation in the long fiber delay line causes a spectral broadening, and also the linewidth enhancement and dispersion influence the instantaneous power spectrum. The broadening is counterbalanced by the bandpass filter, narrowing the spectrum again by the repetitive filtering event at each round trip.

For these investigations, a detailed analysis of the optical field propagation in the FDML laser is presented. The temporal evolution of characteristic spectral parameters at various positions in the cavity, such as the frequency shift and the linewidth, is investigated, yielding the described insight into the formation of a steady state light field. All relevant physical

effects are considered in our model. A comparison of numerical results to experimental data shows good agreement, validating the theoretical model. These new insights represent an important step toward understanding the fundamental mechanisms governing the steady state dynamics in the FDML regime, and are helpful toward a further optimization of the FDML laser.

ACKNOWLEDGMENTS

S. Todor and C. Jirauschek acknowledge support from Professor P. Lugli at the TUM. Their work was supported by the German Research Foundation (DFG) within the Emmy Noether program (JI 115/1-1) and under DFG Grant No. JI 115/2-1. S. Todor additionally acknowledges support from the TUM Graduate School. B. Biedermann and R. Huber would like to acknowledge support from Professor W. Zinth at the LMU Munich. Their work was supported by the German Research Foundation (DFG) within the Emmy Noether program (HU 1006/2-1), by the European Union project FUN OCT (FP7 HEALTH, Contract No. 201880) and the ERC Starting Grant FDML-Raman (FP7 ERC, Contract No. 259158).

REFERENCES

1. D. Huang, E. A. Swanson, C. P. Lin, J. S. Schuman, W. G. Stinson, W. Chang, M. R. Hee, T. Flotte, K. Gregory, C. A. Puliafito, and J. G. Fujimoto, "Optical coherence tomography," Science **254**, 1178–1181 (1991).
2. S. Yun, G. Tearney, Johannes de Boer, N. Iftimia, and B. Bouma, "High-speed optical frequency-domain imaging," Opt. Express **11**, 2953–2963 (2003).
3. L. A. Kranendonk, X. An, A. W. Caswell, R. E. Herold, S. T. Sanders, R. Huber, J. G. Fujimoto, Y. Okura, and Y. Urata, "High speed engine gas thermometry by Fourier-domain mode-locked laser absorption spectroscopy," Opt. Express **15**, 15115–15128 (2007).
4. R. Huber, M. Wojtkowski, K. Taira, J. G. Fujimoto, and K. Hsu, "Amplified, frequency swept lasers for frequency domain reflectometry and OCT imaging: design and scaling principles," Opt. Express **13**, 3513–3528 (2005).
5. R. Huber, M. Wojtkowski, and J. G. Fujimoto, "Fourier domain mode locking (FDML): A new laser operating regime and applications for optical coherence tomography," Opt. Express **14**, 3225–3237 (2006).
6. R. Huber, D. C. Adler, and J. G. Fujimoto, "Buffered Fourier domain mode locking: unidirectional swept laser sources for optical coherence tomography imaging at 370,000 lines/s," Opt. Lett. **31**, 2975–2977 (2006).
7. W. Wieser, B. R. Biedermann, T. Klein, C. M. Eigenwillig, and R. Huber, "Multi-megahertz OCT: high quality 3D imaging at 20 million A-scans and 4.5 GVoxels per second," Opt. Express **18**, 14685–14704 (2010).
8. T. Klein, W. Wieser, C. M. Eigenwillig, B. R. Biedermann, and R. Huber, "Megahertz OCT for ultrawide-field retinal imaging with a 1050 nm Fourier domain mode-locked laser," Opt. Express **19**, 3044–3062 (2011).
9. D. Derickson, M. Bernacil, A. DeKelaita, B. Maher, and S. O'Connor, "SGDBR single-chip wavelength tunable lasers for swept source OCT," Proc. SPIE **6847**, 68472P (2008).
10. S. H. Yun, C. Boudoux, G. J. Tearney, and B. E. Bouma, "High-speed wavelength-swept semiconductor laser with a polygon-scanner-based wavelength filter," Opt. Lett. **28**, 1981–1983 (2003).
11. R. Huber, M. Wojtkowski, J. G. Fujimoto, J. Y. Jiang, and A. E. Cable, "Three-dimensional and C-mode OCT imaging with a compact, frequency swept laser source at 1300 nm," Opt. Express **13**, 10523–10538 (2005).
12. E. C. Vail, M. S. Wu, G. S. Li, L. Eng, and C. J. Chang-Hasnain, "GaAs micromachined widely tunable Fabry-Perot filters," Electron. Lett. **31**, 228–229 (1995).
13. D. C. Adler, W. Wieser, F. Trepanier, J. M. Schmitt, and R. A. Huber, "Extended coherence length Fourier domain mode locked lasers at 1310 nm," Opt. Express **19**, 20930–20939 (2011).
14. V. J. Srinivasan, D. C. Adler, Y. L. Chen, I. Gorczynska, R. Huber, J. S. Duker, J. S. Schumann, and J. G. Fujimoto, "Ultrahigh-speed optical coherence tomography for three-dimensional and en face imaging of the retina and optic nerve head," Investig. Ophthalmol. Vis. Sci. **49**, 5103–5110 (2008).
15. D. C. Adler, Y. Chen, R. Huber, J. Schmitt, J. Connolly, and J. G. Fujimoto, "Three-dimensional endomicroscopy using optical coherence tomography," Nat. Photon. **1**, 709–716 (2007).
16. K. Hsu, P. Meemon, K. S. Lee, P. J. Delfyett, and J. P. Rolland, "Broadband Fourier-domain mode-locked lasers," Photon. Sens. **1**, 222–227 (2011).
17. G. Y. Liu, A. Mariampillai, B. A. Standish, N. R. Munce, X. Gu, and I. A. Vitkin, "High power wavelength linearly swept mode locked fiber laser for OCT imaging," Opt. Express **16**, 14095–14105 (2008).
18. Y. Mao, C. Flueraru, S. Sherif, and S. Chang, "High performance wavelength-swept laser with mode-locking technique for optical coherence tomography," Opt. Commun. **282**, 88–92 (2009).
19. M. Y. Jeon, J. Zhang, and Z. P. Chen, "Characterization of Fourier domain mode-locked wavelength swept laser for optical coherence tomography imaging," Opt. Express **16**, 3727–3737 (2008).
20. M. Y. Jeon, J. Zhang, Q. Wang, and Z. Chen, "High-speed and wide bandwidth Fourier domain mode-locked wavelength swept laser with multiple SOAs," Opt. Express **16**, 2547–2554 (2008).
21. E. J. Jung, C. S. Kim, M. Y. Jeong, M. K. Kim, M. Y. Jeon, W. Jung, and Z. Chen, "Characterization of FBG sensor interrogation based on a FDML wavelength swept laser," Opt. Express **16**, 16552–16560 (2008).
22. Y. Wang, W. Liu, J. Fu, and D. Chen, "Quasi-distributed fiber Bragg grating sensor system based on a Fourier domain mode locking fiber laser," Laser Phys. **19**, 450–454 (2009).
23. D. Chen, C. Shu, and S. He, "Multiple fiber Bragg grating interrogation based on a spectrum-limited Fourier domain mode-locking fiber laser," Opt. Lett. **33**, 1395–1397 (2008).
24. L. Kirsten, J. Walther, P. Cimalla, M. Gaertner, S. Meissner, and E. Koch, "Optical coherence tomography for imaging of subpleural alveolar structure using a Fourier domain mode locked laser," Proc. SPIE **8091**, 809118 (2011).
25. B. C. Lee and M. Y. Jeon, "Remote fiber sensor based on cascaded Fourier domain mode-locked laser," Opt. Commun. **284**, 4607–4610 (2011).
26. B. C. Lee, E. J. Jung, C. S. Kim, and M. Y. Jeon, "Dynamic and static strain fiber Bragg grating sensor interrogation with a 1.3 mu m Fourier domain mode-locked wavelength-swept laser," Meas. Sci. Technol. **21**, 094008 (2010).
27. E. J. Lee and Y. P. Kim, "Swept source optical coherence tomography with external clocking using voltage controlled oscillator," Opt. Eng. **50**, 053205 (2011).
28. M. T. Tsai, H. L. Liu, F. Y. Chang, T. C. Chang, and C. H. Yang, "Three-dimensional and en-face optical coherence tomography based on a Fourier domain mode locking laser for dermatology study," in *First International Symposium on Bioengineering* (Research Publishing Services, 2011), pp. 88–95.
29. S. Moon and D. Y. Kim, "Ultra-high-speed optical coherence tomography with a stretched pulse supercontinuum source," Opt. Express **14**, 11575–11584 (2006).
30. C. M. Eigenwillig, B. R. Biedermann, W. Wieser, and R. Huber, "Wavelength swept amplified spontaneous emission source," Opt. Express **17**, 18794–18807 (2009).
31. C. M. Eigenwillig, T. Klein, W. Wieser, B. R. Biedermann, and R. Huber, "Wavelength swept amplified spontaneous emission source for high speed retinal optical coherence tomography at 1060 nm," J. Biophotonics **4**, 552–558 (2011).
32. T. Yano, H. Saitou, N. Kanbara, R. Noda, S. I. Tezuka, N. Fujimura, M. Ooyama, T. Watanabe, T. Hirata, and N. Nishiyama, "Wavelength modulation over 500 kHz of micromechanically tunable InP-based VCSELs with Si-MEMS technology," IEEE J. Quantum Electron. **15**, 528–534 (2009).
33. V. Jayaraman, J. Jiang, H. Li, P. Heim, G. Cole, B. Potsaid, J. G. Fujimoto, and A. Cable, "OCT imaging up to 760 kHz axial scan rate using single-Mode 1310 nm MEMS-tunable VCSELs with

>100 nm tuning rate," in *Quantum Electronics and Laser Science Conference* (Optical Society of America, 2011).

34. G. Overton, "760 kHz OCT scanning possible with MEMS-tunable VCSEL," Laser Focus World **47**, 15 (2011).
35. W.-Y. Oh, B. J. Vakoc, M. Shishkov, G. J. Tearney, and B. E. Bouma, ">400 kHz repetition rate wavelength-swept laser and application to high-speed optical frequency domain imaging," Opt. Lett. **35**, 2919–2921 (2010).
36. C. Jirauschek, B. Biedermann, and R. Huber, "A theoretical description of Fourier domain mode locked lasers," Opt. Express **17**, 24013–24019 (2009).
37. S. Todor, B. Biedermann, W. Wieser, R. Huber, and C. Jirauschek, "Instantaneous lineshape analysis of Fourier domain mode-locked lasers," Opt. Express **19**, 8802–8807 (2011).
38. B. R. Biedermann, W. Wieser, C. M. Eigenwillig, T. Klein, and R. Huber, "Direct measurement of the instantaneous linewidth of rapidly wavelength-swept lasers," Opt. Lett. **35**, 3733–3735 (2010).
39. G. P. Agrawal, *Nonlinear Fiber Optics* (Academic, 2001).
40. C. H. Henry, "Theory of the linewidth of semiconductor-lasers," IEEE J. Quantum Electron. **18**, 259–264 (1982).
41. A. Bilenca, S. H. Yun, G. J. Tearney, and B. E. Bouma, "Numerical study of wavelength-swept semiconductor ring lasers: the role of refractive-index nonlinearities in semiconductor optical amplifiers and implications for biomedical imaging applications," Opt. Lett. **31**, 760–762 (2006).